Lighting-Up Two-Dimensional Lanthanide Phosphonates: Tunable Structure-Property Relationships towards Visible and Near-Infrared Emitters

Adam R. Patterson, Wolfgang Schmitt* and Rachel C. Evans*

School of Chemistry and CRANN, The University of Dublin, Trinity College, Dublin 2, Ireland.

* Corresponding authors: E-mail: schmittw@tcd.ie; Tel: +353 1 896 3495, E-mail: raevans@tcd.ie; Tel: +353 1 896 4215

ABSTRACT

We report the solvothermal synthesis and characterization of the structure, morphology and photoluminescence properties of a series of unprecedented layered, organic-inorganic lanthanide (Ln^{III}) phosphonates based on *t*-butyl- (Bu^t), 1-naphthalene- (Naph) and 4-biphenyl- (Biphen) phosphonic acid. Through systematic variation of the ligand and the Ln^{III}, we discuss the key structure-property relationships that must be managed for the design of Ln-phosphonates with tailored functionality. Single crystal and X-ray powder diffraction studies revealed the size and shape of the employed ligand affects the type of layered material that forms. In agreement with their molecular structures two distinct crystal morphologies are observed, 1D nanorods and 2D platelets, demonstrating that the anisotropy in the crystal structure and the variable coordination behavior of the ligands is directly translated to the crystal growth. Judicious selection of the ligand enables us to switch-on Ln-centred photoluminescence in both the visible (Eu^{III}, Tb^{III}) and near infrared (Nd^{III} and Yb^{III}) spectral regions. Notably, the presented Yb-phosphonates are rare examples of phosphonate-based near infrared emitters. Furthermore, the Eu^{III} spectral fingerprint provided unique insight into

the coordination environment of the metal center, facilitating structural characterization where X-ray diffraction analysis was limited.

1. Introduction

Coordination-based multidimensional hybrids constructed from organic and inorganic building blocks have emerged as an important class of functional materials due to their potential applications in catalysis, ion exchange, gas sorption and intercalation chemistry.[1,2] In recent years, two-dimensional (2D) materials have attracted significant interest due to the fascinating properties that arise from the anisotropic molecular structure.[3-11] Although, purely inorganic materials, for example graphene[3-5], MoS_2[6-8], BN[9,10] and GaN[11], have been intensively studied, the related 2D organic-inorganic systems have been largely overlooked. Metal phosphonates, in which the phosphonate oxygen atoms coordinate strongly to the metal ions, forming two-dimensional inorganic layers separated by the hydrophobic regions of the organic moieties, offer considerable potential in this regard.[12-19] The remarkable coordination ability of phosphonates has frequently been exploited in diverse industrial technologies (e.g. corrosion inhibitors, waste water management and heterogeneous catalysis).[20-22] Lanthanide (Ln^{III}) phosphonates are particularly intriguing, since they fuse the high coordination number of the lanthanide centre with the variable binding modes of the phosphonate, which can lead to layered topologies.[23-27] Moreover, Ln^{3+}-based materials often exhibit intense room temperature photoluminescence (PL) across the UV to near-IR spectral range, arising from *f-f* electronic transitions.[28-30] This expands the potential applications of lanthanide phosphonates to optoelectronic devices, solid-state lighting, sensing and optical communications and storage.[29,31-34]

When combined with a metal center, monofunctional organophosphonate ligands generally result in the formation of layered materials.[1,23] Judicious selection of the metal center and ligand should enable the isolation of lanthanide phosphonate hybrids exhibiting well-defined 2D structures with tailored optical properties. However, the design and characterization of these materials can be challenging, since lanthanide phosphonates

typically exhibit low solubility and poor crystallinity.[35] Additional functionalization of the phosphonic acid ligand (*e.g.* with carboxylate[36-39], hydroxyl[40,41], amine[42,43] or crown ether groups[44,45]) has been shown improve both the solubility and crystallinity of these materials. Moreover, direct population of the Ln^{III} excited states is limited by the low molar absorption coefficients (1-10 dm^3 mol^{-1} cm^{-1}) associated with Laporte-forbidden *f-f* transitions.[46] Sensitization of the Ln^{III} emissive state *via* energy transfer from an aromatic organic chromophore can be used to circumvent this obstacle.[47] This so-called *antenna effect* has been exploited extensively to modify the optical properties of lanthanide complexes[48,49], lanthanide-organic frameworks (LnOFs)[50,51], and more recently lanthanide phosphonates.[38,52,53] Understanding and controlling the interdependent relationships that determine each of these factors will therefore be a crucial step forward in enabling the strategic design of functional lanthanide phosphonates.

Recently, several studies probing the structure, morphology and optical properties of lanthanide phenyl phosphonates prepared from the reaction with phenyl phosphonic acid have been reported.[23] Ma and coworkers demonstrated that addition of sodium *p*-toluene sulfonate to the reaction mixture under hydrothermal conditions promoted preferential growth of one-dimensional nanorods.[54] Comparison of Eu^{III} and La^{III}/Eu^{III} phenyl phosphonate nanorods against the corresponding bulk materials revealed that crystal size has only a negligible effect on the PL properties. Pinna *et al.* have since shown that changing from an aqueous to non-aqueous synthetic route can greatly enhance the photoluminescence quantum yields (Φ_{PL}) of the Eu^{III}-doped lanthanum phenyl phosphonate, reporting an impressive value Φ_{PL}=45% for $La(HO_3PC_6H_5)_2$:0.06Eu *via* ligand sensitization.[55] The improved PL efficiency is attributed to a combination of reduced concentration quenching *via* co-doping with La^{III} and inhibition of non-radiative multiphonon relaxation *via* O-H oscillators through the use of an organic solvent. Pinna *et al.* further demonstrated that citric acid can act as a crystal habit-

modifier for the related $YH(O_3PC_6H_5)_2$:Ln0.05 (Ln = Eu^{III}, Tb^{III}), promoting the formation of dandelion-like superstructures composed of multiple individual nanorods.[56] Notably, a ~50% increase in the Φ_{PL} of $YH(O_3PC_6H_5)_2$:Ln0.05 could be obtained in moving from plate-like to dandelion-like morphologies. It is clear from these initial studies that the chemical composition, morphology and optical properties of these materials are closely linked; an understanding the specific nature of this relationship, however, remains elusive.

Here we adopt a strategic approach to the design and synthesis of layered lanthanide phosphonates with targeted morphology and optical properties. We have carefully selected three ligands, namely *t*-butyl-, 1-naphthalene- and 4-biphenyl phosphonic acid (Table 1), which will allow us to selectively probe the effect of ligand size on the interlamellar spacing of the corresponding lanthanide phosphonates. Moreover, 1-naphthalene- and 4-biphenyl phosphonic acid were judiciously chosen on the basis of the energy of their excited electronic states and their high molar absorption coefficients, and are expected to efficiently sensitize the emissive Ln^{III} state. By varying the Ln^{III} ion we were able to tune the emission wavelength from green (Tb^{III}), to the red (Eu^{III}), to the near-IR (Nd^{III}, Yb^{III}) and simultaneously investigate the effect of the ligand type and size, and the metal ionic radius, on the morphology of the material. To the best of our knowledge, this is the first study pertaining to lanthanide phosphonates to take a global consideration of both the electronic properties and size of the constituent organic and inorganic building blocks in tandem. Notably we observe room-temperature emission from a simple, layered ytterbium phosphonate (based on 1-naphthalene- and 4-biphenyl phosphonic acid) for the first time.

2. Experimental Section

2.1 Synthesis of lanthanide phosphonates. Lanthanide phosphonates were prepared using a solvothermal route. In a typical synthesis, a mixture of ligand (0.4 mmol), $LnCl_3 \cdot 6H_2O$ (0.2

mmol, Ln = Nd^{III}, Eu^{III}, Tb^{III} and Yb^{III}) and an appropriate solvent (5 mL) were placed in a 20 mL Teflon liner and stirred for 30 minutes to give a white cloudy suspension. The pH was adjusted to 2 using 1 M NaOH aqueous solution. The Teflon liner was inserted into a steel autoclave and placed in an oven at 100 °C for 48 hours. Following cooling to room temperature, the resulting material was filtered and washed with water and ethanol before drying at 80 °C. The ligands investigated were *t*-butyl phosphonic acid (Bu^t), 1-naphthalene phosphonic acid (Naph) and 4-biphenyl phosphonic acid (Biphen). Ligand structures, the composition of the Ln phosphonates prepared and the corresponding sample names are shown in Table 1. Complete synthetic procedures and characterization data for all samples investigated may be found in the Supporting Information.

2.2 Characterization. Single crystal X-ray crystallography of **Eu-Bu^t** was performed at 108 K on a Rigaku Saturn-724 diffractometer using graphite monochromated Mo Kα radiation. The omega scan method was used to collect a full sphere of data. Data was collected, processed and corrected for absorption and polarization effects using the Crystalclear SM 1.4.0 software. The structure was solved using direct methods and refined using the SHELXTL program.[57] The crystallographic details and refinement parameters are provided in the Supporting Information; the crystallographic data can be obtained free of charge for the Cambridge Crystallographic Data Centre (CCDC, No: 980771). Powder X-ray diffraction (PXRD) was performed using a Siemens D500 diffractometer using Cu Kα radiation. All diffraction patterns were measured in the 2θ range 2-70° using a 0.02° step size and 14.7 s counting rate.

Fourier transform infrared (FTIR) spectra were measured using a PerkinElmer Spectrum 100 FTIR spectrometer in the range 4000-650 cm^{-1}. Solution NMR spectroscopy was performed on a Bruker DPX 400 NMR machine. ^{1}H and ^{31}P spectra were obtained at 400 and 162 MHz, respectively. Electrospray mass spectrometry (MS) was performed on a

Micromass LCT Electrospray mass spectrometer. Samples were dissolved in a suitable HPLC grade solvent. Thermogravimetric analysis (TGA) was performed on a Perkin Elmer Pyris 1 TGA thermogravimetric analyzer in the range 30-900 °C in an air atmosphere using a heating rate of 10 °C/min. Elemental analyses (CHN) were performed in the Microanalysis Lab of the School of Chemistry and Chemical Biology, University College Dublin.

Solution-state UV/Vis absorption spectroscopy was performed on a Shimadzu UV-2401 PC spectrometer using matched quartz cuvettes (path length 10 mm). Solid-state UV-Vis diffuse reflectance spectroscopy was performed on a Perkin Elmer Lambda 1050 spectrometer using an integrating sphere accessory across the range 250-800 nm.

Steady-state photoluminescence spectroscopy was performed on a Fluorolog-3 spectrophotometer (Horiba Jobin Yvon), using the front-face configuration for solid state samples. Low temperature phosphorescence measurements on the ligands naphthalene phosphonic acid and biphenyl phosphonic acid were performed at 77 K using a liquid nitrogen filled quartz dewar. Spectra measured in the UV/Vis range used a room temperature R9281x photomultiplier tube as the detector. Near-Infrared (NIR) spectra were measured using a liquid nitrogen cooled R5509 photomultiplier tube as the detector. Emission and excitation spectra were corrected for the wavelength response of the system and the intensity of the lamp profile over the excitation range, respectively, using correction factors supplied by the manufacturer. Absolute photoluminescence quantum yields (Φ_{PL}) were measured using an F-3018 integrating sphere accessory (Horiba Jobin Yvon). Three measurements for each sample were taken and the average value is reported. The method has an error margin of 10%. Emission lifetimes in the visible region were measured using a Jobin-Yvon Fluorolog 3-22 equipped with a Spex 1934D phosphorimeter accessory. Emission decay curves were fit to either a single or double exponential decay function in Origin 8.0 data analysis program.

Samples for scanning electron microscopy (SEM) were prepared by drop-casting the sample onto silicon wafers. The wafer was mounted onto a carbon disc and a connection made between wafer and stage use Ag-DAG paint. SEM images were recorded on a Zeiss-Ultra Scanning Electron Microscope at an accelerating voltage of 2 kV. Energy dispersive spectroscopy (EDS) was carried out using an Oxford Instruments INCA system attached to the microscope.
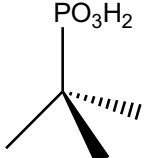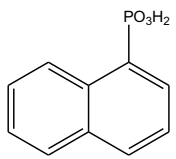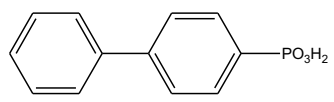
3. Results

3.1 Synthesis, structure and composition. Lanthanide phosphonate organic-inorganic hybrids were prepared from the reaction of a two to one mole ratio of ligand to Ln(III) chloride (Ln = Nd^{III}, Eu^{III}, Tb^{III} and Yb^{III}) under solvothermal conditions at 100 °C. Hybrids prepared using t-butyl phosphonic acid were reacted in acetonitrile (**Ln-Bu^t**), whilst reactions of 1-naphthalene- and 4-biphenyl-phosphonic acid (**Ln-Naph** and **Ln-Biphen**, respectively) were performed in deionized water, to produce crystalline powders of the coordination compounds. Sample names, compositions and ligand structures are summarized in Table 1.

The Fourier transform infrared (FTIR) spectra of all Ln-phosphonates prepared display characteristic stretching modes associated with the deprotonated phosphonic acid group (Figure S1, Supporting Information), namely ν_{P-O} at ~1000 cm^{-1} and 1100 cm^{-1}, $\nu_{P=O}$ at 1600 cm^{-1} and ν_{P-C} at 1400 cm^{-1}.[55] Typical C-H (~3000 cm^{-1}) and C=C stretching modes (~1600 cm^{-1}) associated with the organic ligand are also observed.

**Table 1.** Sample names, compositions and ligand structures of the Ln-phosphonates investigated.

Series	Ligand	Formula
Ln-Bu^t		$[Nd(HO_3PC(CH_3)_3)_3] \cdot H_2O$
		$[Eu(HO_3PC(CH_3)_3)_3] \cdot H_2O$
		$[Tb(HO_3PC(CH_3)_3)_3] \cdot H_2O$
		$[Yb(HO_3PC(CH_3)_3)_3] \cdot H_2O$
Ln-Naph		$[Nd(O_3PC_{10}H_7)_2(H_2O)_2]$
		$[Eu(O_3PC_{10}H_7)_2(H_2O)_2]$
		$[Tb(O_3PC_{10}H_7)_2(H_2O)_2]$
		$[Yb(O_3PC_{10}H_7)_2(H_2O)_2]$
Ln-Biphen		$[Nd(O_3PC_{12}H_9)_2]$
		$[Eu(O_3PC_{12}H_9)_2]$
		$[Tb(O_3PC_{12}H_9)_2]$
		$[Yb(O_3PC_{12}H_9)_2]$

Thermogravimetric analysis (TGA) of the Ln-phosphonates was performed in air (Figure S2, Supporting Information) to establish the chemical composition and thermal stability. The thermogram obtained for **Ln-Bu^t** reveals three gravimetric events: a loss of 3.3% between 50-100 °C due to the loss of the water of crystallization (*calc*. 3.1%) and two subsequent losses at 420-450 °C and 520-580 °C, with a combined 31% weight loss (*calc*. 29.4%), attributed to decomposition and loss of the *t*-butyl moiety. The residual substance is assumed to be a lanthanide phosphate. **Ln-Naph** materials display two gravimetric events: a 6.1% weight loss at 190 °C which is assigned to two coordinated water molecules (*calc*. 6.0%) and a loss centred at 400 °C assigned to the loss of two coordinated naphthalene ligands, yielding $[Ln(O_3PC_{10}H_7)_2(H_2O)_2]$ (*calc*. 43.2-44.3%, *obs*. 40.3% [loss 2 equiv. $C_{10}H_8$ moieties]) as a reasonable empirical formula. A single gravimetric event centred at 500 °C due to decomposition of the organic residues for **Ln-Biphen** indicate two coordinated ligands with formula $[Ln(O_3PC_{12}H_9)_2]$ (*calc*. 49.1%, *obs*. 48.8 % [loss 2 equiv. $C_{12}H_9$ moieties]).

Single crystal X-ray analysis allowed us to determine the detailed molecular arrangement of [$Eu^{III}(HO_3PC(CH_3))_3$]·H_2O (**Eu-Bu^t**), which crystallizes in the monoclinic crystal system in the space group $P2_1/c$. Each Eu^{III} ion coordinates to six organophosphonate ligands to give a distorted octahedral coordination geometry. Each crystallographically distinct organophosphonate Bu^t-PO_3H^- remains partially protonated, whereby only two phosphonate oxygen atoms are free to coordinate. These oxygen donors bridge two Eu^{III} centers to produce 1D polymeric chains that extend along the *c*-axis (Figure 1a). Constitutional water molecules engage in hydrogen bonding, organizing one-dimensional polymer chains into a two-dimensional assembly that extends parallel to the *bc*-plane. This hydrogen bonding between the water molecules and non-coordinating phosphonate oxygen atoms gives rise to a *pseudo*-layered arrangement of intricate pleated-like sheets that stack *via* Van der Waals forces in the direction of the crystallographic *a*-axis. (Figure 1a and b).

The structure of **Eu-Bu^t** has both similarities and differences to that of the lanthanide phenyl phosphonate, [$La(O_3PC_6H_5)(HO_3PC_6H_5)$], reported by Clearfield *et al.*[29] Whilst both compounds adopt layered supramolecular structures which contain distinct inorganic {Eu(III)-O}-based regions that are encapsulated by organic moieties protruding into the interlamellar spacings, they exhibit contrasting coordination behavior due to the differing geometrical requirements of the *tert*-butyl and phenyl ligands.[38,58,59] In [$La(O_3PC_6H_5)(HO_3PC_6H_5)$] the formation of two-dimensional coordination polymer sheets is facilitated by the dodecahedral Ln^{III} environment and bridging oxygen donors.[23] In contrast, in **Eu-Bu^t** the octahedral geometry leads to the formation of one-dimensional chains that assemble *via* hydrogen bonding, which leads to the assembly of pleated-like sheets. Substitution of Eu^{III} by Nd^{III}, Tb^{III} or Yb^{III} leads to a series of four isostructural compounds as confirmed by FTIR spectroscopy and powder XRD (see Figure 2a, Figure S1 and S3).
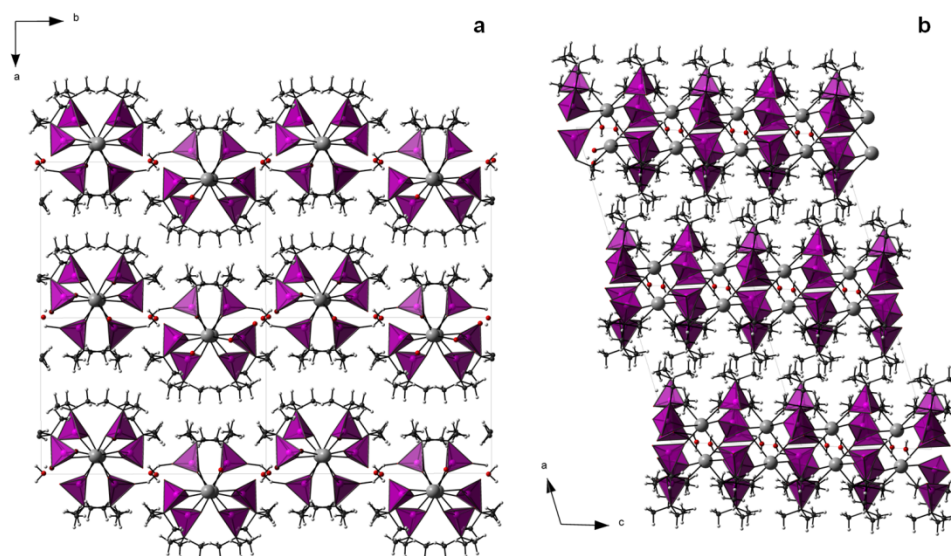
Figure 1. Crystal structure of $[Eu^{III}(HO_3PC(CH_3))_3]\cdot H_2O$, **Eu-Bu^t**. The 3D packing arrangement of 1D polymeric chains as seen down the projection of the (a) *c*-axis and (b) *b*-axis (C:Black, O:Red, P:Pink tetrahedra, Eu:Grey. Blue dashed line represents hydrogen bonding).

The chemical composition of the Ln-Naph series, $[Ln(O_3PC_{10}H_7)_2(H_2O)_2]$, is consistent with that of the structurally-related $[La(O_3PCH_2C_6H_5)_2(H_2O)_2]$, which crystallizes in the orthorhombic space group *Pbcn* with *a* =10.801(2) Å, *b* = 10.301(2) Å and *c* = 33.246(8) Å.[23] Using the PXRD patterns of the Ln-Naph series, the individual reflections were indexed using the program Taup to provide an orthorhombic unit cell with *a* =13.76 Å, *b*=16.42 Å and *c*=23.31 Å. Taking into account systematic absences, the centrosymmetric space group, *Pcca*, was assigned. In a similar fashion, the PXRD pattern of **Ln-Biphen** has been indexed to provide a monoclinic unit cell, with dimensions *a*=23.80 Å, *b*=6.75 Å and *c*=5.34 Å with *β*=92.95°.

Figure 2b shows representative PXRD patterns for **Eu-Bu^t**, **Eu-Naph** and **Eu-Biphen**, which all exhibit intense periodic reflections originating from their layered lamellar structures that are characteristic for organophosphonate-stabilized lanthanide coordination compounds.[54-56] The interlayer spacing, *d*, as determined from Bragg's law is directly

proportional to the ligand size, following the order **Ln-Bu^t** (12.27 Å ± 0.01) < **Ln-Naph** **(**16.38 Å ± 0.01) < **Ln-Biphen** (23.64 Å ± 0.01).
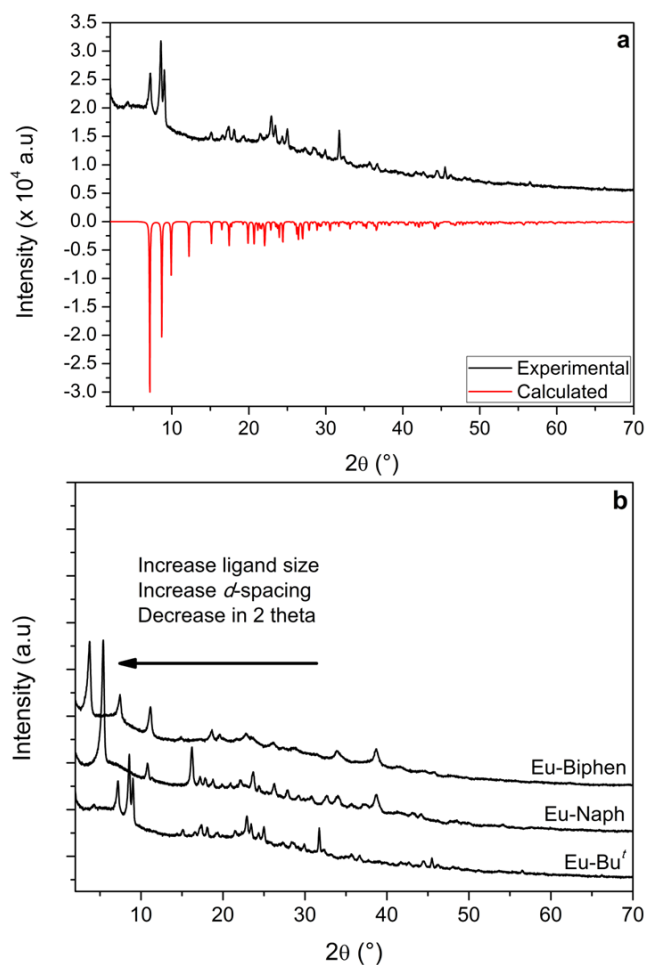
Figure 2. (a) Experimental and calculated PXRD patterns for **Eu-Bu^t**, (b) comparison of PXRD patterns for the different Eu-phosphonates showing the variation in *d*-spacing with changing ligand

3.2 Morphology. A Scanning Electron Microscopy (SEM) study was undertaken to investigate the effect of ligand size and ionic radii on the morphologies of these materials (Figure 3). In general, the layered molecular structure is represented in the morphology and we observe platelet-type crystals of sub-micrometer dimensions for all samples. Notably, the Yb-based organophosphonates show a tendency towards anisotropic crystal growth to form

rods whose aspect ratio is influenced by the nature of the organic ligand. This may in part be attributable to the smaller ionic radius of the Yb^{III} ion compared to the other Ln^{III} investigated.[60] Addition of the STS habit modifier improves the monodispersity of these 1D rod materials. Moreover, in agreement with our crystallographic analysis, all Ln-Bu^t exhibit rod-like crystal morphologies providing further evidence for a *pseudo*-2D structure that is assembled from 1D coordination polymers. The Ln-Biphen series gives rise to film-like assemblies (Fig 3f), whose amorphous character is consistent with the corresponding PXRD patterns (Figure 2b).
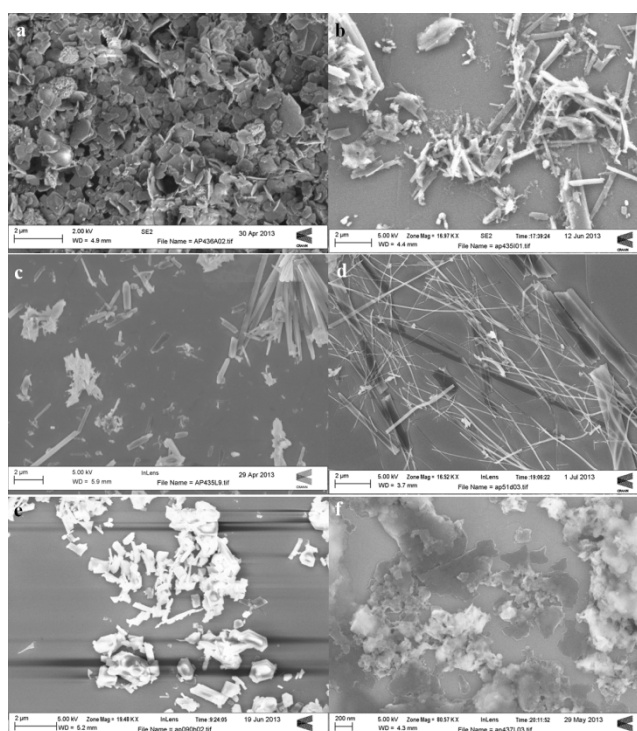
Figure 3. SEM images of (a) platetlets of **Nd-Naph** (no *p*-STS), (b) rod structures of **Yb-Naph** amongst some nanoparticles (no *p*-STS), (c) phase pure rod structures of **Yb-Naph** (with *p*-STS), (d) rod structures of **Yb-Bu^t** and (e) **Nd-Bu^t** and (f) film-like assemblies of **Yb-Biphen** (with *p*-STS modifier) .

3.3 Photoluminescence (PL) properties. Figures 4b and 4c show the PL and excitation spectra of **Eu-Bu^t**, **Eu-Naph** and **Eu-Biphen**. On direct excitation of the Eu^{III} centre (λ_{ex} = 393 nm, $^7F_0 \rightarrow ^5L_6$) (Figure 4b, S5), characteristic Eu^{III}-centred red photoluminescence originating from $^5D_0 \rightarrow ^7F_J$ transitions (J = 0-4) between 570-720 nm is observed for all samples (e.g. see Fig 4a). Emission from higher excited states (*e.g.* $^5D_1$) is not observed indicating efficient non-radiative relaxation to the $^5D_0$ manifold. The characteristic Eu^{III} emission spectrum is also obtained for **Eu-Naph** and **Eu-Biphen** *via* ligand sensitization (λ_{ex} = 320 nm and λ_{ex} = 305 nm (Figure 4b), respectively). For both metal-centered and ligand excitation, the most intense transition is the hypersensitive $^5D_0 \rightarrow ^7F_2$ emission line, which is common for eight-coordinate lanthanide centers.[61] The absence of ligand-centered emission in the PL spectrum (Figure S6) suggests that energy transfer from the ligand to the metal center is very efficient. The corresponding excitation spectra (monitored in the $^5D_0 \rightarrow ^7F_2$ transition) exhibit characteristic metal-centered *ff* emission lines corresponding to transitions between the $^7F_0$ ground state and the $^5D_{4-1}$, $^5G_{2-6}$ and $^5L_6$ excited states (Figure 4c). In addition, **Eu-Naph** and **Eu-Biphen** display broad excitation bands centred at 320 nm and 300 nm. Comparison with the UV/Vis absorption spectra of the free ligands (Figure S7, Supporting Information) confirms that these bands result from ligand-based excitation.
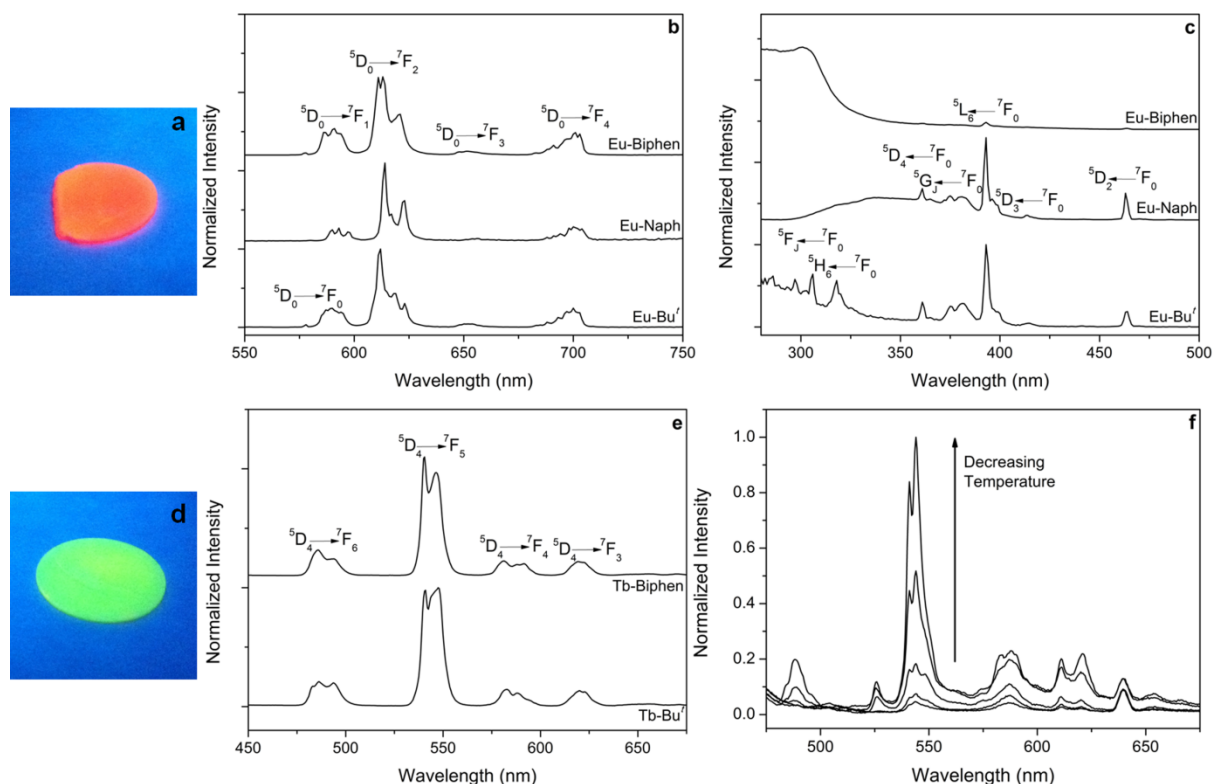
Figure 4. (a, d) Photographs of **Eu-Biphen** and **Tb-Biphen** under excitation with a UV-lamp (b) Room-temperature (RT) PL spectra for **Eu-Bu^t** obtained upon direct excitation at 393 nm ($^5L_6 \leftarrow {}^7F_0$) and **Eu-Naph** and **Eu-Biphen** on ligand excitation (λ_{ex} = 320 nm and λ_{ex} = 305 nm, respectively). (c) Corresponding RT excitation spectra (λ_{em} = 610-614 nm, $^5D_0 \rightarrow {}^7F_2$ transition). (e) RT PL spectra for **Tb-Bu^t** obtained upon direct excitation at 377 nm ($^5D_3 \leftarrow {}^7F_6$) and **Tb-Biphen** on ligand excitation (λ_{ex} = 305 nm). (f) Low temperature (77-250 K) PL spectra for **Tb-Naph** upon ligand sensitization (λ_{ex} = 320 nm).

The ground ($^7F_0$) and the emissive ($^5D_0$) states of Eu^{III} are nondegenerate and cannot be split by the crystal field.[29] As such, there is a one-to-one correspondence between the number of bands associated with the $^5D_0 \rightarrow {}^7F_0$ transition in the PL spectrum and the number of distinct Eu^{III} environments.[29,62] Gaussian deconvolution of this band reveals a single Eu^{III} local environment for all Eu-phosphonates, which is in good agreement with the crystallographic data.

The PL and excitation spectra for **Tb-Bu^t** and **Tb-Biphen** are shown in Figures 4e and S8. Characteristic Tb[III]–centered green emission is observed in the range of 450-700 nm corresponding to $^5D_4 \rightarrow {^7F_J}$ (J = 6-2) transitions upon direct excitation of the metal center (see Figure 4d). The excitation spectra for **Tb-Bu^t** display characteristic *ff* transitions between 300-500 nm, corresponding to transitions from the $^7F_6$ ground state to the $^5D_{4\text{-}3}$, $^5L_{10}$ and ^5G_J excited states. Ligand sensitization of the Tb[III] photoluminescence is also observed for **Tb-Biphen** (Figure 4e and S6d, Supporting Information). The relative intensity of the observed PL is significantly greater (under the same experimental conditions) than for direct excitation of the same sample, suggesting that efficient ligand to metal energy transfer occurs. This is supported by the dominance of the broad ligand band in the excitation spectrum (monitored in the $^5D_4 \rightarrow {^7F_5}$ transition, Fig. S8a), which obscures the weak *ff* transition lines.

Unexpectedly, no photoluminescence was observed for **Tb-Naph,** for either metal-centered excitation and ligand sensitization at room temperature. However, characteristic Tb[III] emission was observed at 77-250 K, with the relative PL intensity increasing as the temperature decreased (Figure 4f). The excitation spectrum for **Tb-Naph** observed at 77 K (Figure S8b, Supporting Information) is dominated by a ligand-centered band at 320 nm and a weaker emission line centred at 377 nm attributed to the $^5D_3 \leftarrow {^7F_6}$ transition.

Notably, NIR photoluminescence from both Nd[III]- and Yb[III] phosphonates was observed at room temperature. For **Nd-Bu^t**, **Nd-Naph** and **Nd-Biphen**, characteristic Nd[III] emission lines assigned to the $^4F_{3/2} \rightarrow {^4I_{J/2}}$ (J = 13, 11, 9) transitions are observed for direct Nd[III] excitation (λ_{ex} = 580nm, $^5G_{5/2} \leftarrow {^4F_{9/2}}$) (Figure 5a), with **Nd-Biphen** exhibiting some fine splitting for these transitions. Ligand sensitization of the emission is also observed for **Nd-Naph** and **Nd-Biphen** (Figure 5a). The excitation spectra of **Nd-Bu^t** monitored for the $^4F_{3/2} \rightarrow {^4I_{11/2}}$ transition ($\lambda_{em} \sim 1060$ nm) exhibit Nd[III]-centred excitations in the UV to visible range of the spectrum arising from the $^4I_{9/2}$ ground state to the $^4D_{J/2}$, $^4I_{11/2}$, $^2L_{15/2}$, $^2D_{5/2}$, $^2P_{1/2}$,

$^2K_{15/2}$, $^4G_{7/2-5/2}$, $^4S_{3/2}$ and $^4F_{9/2-7/2}$ excited states (Figure 5b). The excitation spectra for **Nd-Naph** and **Nd-Biphen** also display broad bands at 320 and 305 nm due to absorption by the aromatic ligand antenna (Figure 5b). Similar characteristics are observed in the corresponding UV/Vis diffuse reflectance spectra (Figure S9, Supporting Information).
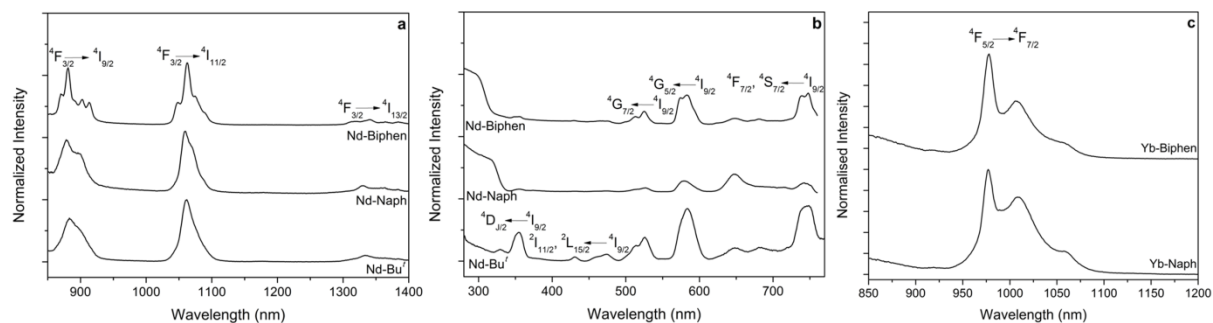
Figure 5. (a) Room-temperature (RT) PL spectra for **Nd-Bu^t** obtained upon direct excitation at 584 nm ($^5G_{5/2} \leftarrow {}^4F_{9/2}$) and **Nd-Naph** and **Nd-Biphen** on ligand excitation (λ_{ex} = 320 nm and λ_{ex} = 305 nm respectively). (b) Corresponding RT excitation spectra (λ_{em} = 1057-1061 nm, $^4F_{3/2} \rightarrow {}^4I_{11/2}$ transition). (c) RT PL spectra for **Yb-Naph** and **Yb-Biphen** under ligand excitation (λ_{ex} = 320 nm and λ_{ex} = 305 nm respectively).

Figure 5c shows the PL spectra for **Yb-Naph** and **Yb-Biphen** obtained upon ligand-centered excitation at 320 and 300 nm, respectively. A broad band centred at 977-978 nm corresponding to the $^4F_{5/2} \rightarrow {}^4F_{7/2}$ transition is observed. The excitation spectra support this observation for **Yb-Naph** and **Yb-Biphen** where there is absorption from the ligand at 320 and 300 nm, respectively, but no ff transitions are observed (Figure S10, Supporting Information).

Photoluminescence quantum yields (Φ_{PL}) for direct excitation of Eu^{III} were ~1-3% for all samples (Table 2). These low values are consistent for direct lanthanide excitation due to the low molar absorption coefficients of the ff transitions.[29] Whilst **Tb-Biphen** and **Tb-Naph** are only weakly or non-emissive at room temperature upon direct excitation of Tb^{III}, the Φ_{PL} for

Tb-Bu^t was significantly greater at 8%. The observed emission lifetimes of Eu^{III} ($^5D_0$) and Tb^{III} ($^5D_4$) phosphonates are shown in Table 2. Upon direct excitation and ligand sensitization **Eu-Naph** exhibits a monoexponential decay curve, with an observed lifetime of τ~0.36 ms. **Eu-Biphen** and **Eu-Bu^t** both exhibit biexponential decay curves, comprised of a short-lived component of similar magnitude (τ_1~0.30-0.38 ms) and a longer lived component of τ_2~1.00-1.32 ms, depending on the mode of excitation. Notably for **Eu-Bu^t** the long-lived component makes only a minor contribution (~7%), but becomes the dominant feature for **Eu-Biphen** (~73%). **Tb-Biphen** and **Tb-Bu^t** similarly exhibit biexponential decay curves, but the lifetime and contribution of each component differs significantly. **Tb-Bu^t** displays two lifetimes, τ_1 ~0.98 ms and τ_2 ~2.69 ms that contribute equally to the decay curve. In contrast, **Tb-Biphen** exhibits two much shorter lived components of similar magnitude that also contribute equally (τ_1 ~0.33 and τ_2 ~0.80 ms). The origin of the biexponential nature of the **Ln-Bu^t** and **Ln-Biphen** is unclear. The crystallographic data indicates that only one Ln^{III} environment is present in all samples. Concentration quenching, where excitation energy migrates between Ln^{III} sites before being trapped by a quencher site is common in solid-state materials where the Ln^{III} concentration exceeds more than a few percent, as is the case here.[64] The observed biexponential decays could therefore arise due to emission from quenched (short-lived) and unquenched sites (longer lived). Moreover, concentration quenching typically results in low emission quantum yields, which is in agreement with our observed values. Non-radiative energy transfer is highly dependent both on the dimensionality and the distance between energy donor and acceptor sites.[30] As such, differences in rate of energy transfer processes occurring within the 2D sheets for **Ln-Biphen** or 1D chains for **Ln-Bu^t** compared to the bulk 3D network are anticipated to lead to complex decay kinetics that deviate from simple exponential behavior. The emission quantum yields for ligand sensitization (Φ_{LS}) can be estimated for Eu^{III} from the experimental lifetimes and the

corrected emission spectrum due to the presence of the purely magnetic $^5D_0\rightarrow^7F_1$ transition, from:[63]

$$\Phi_{\text{LS}} = \frac{k_r}{k_r+k_{nr}} = \frac{\tau_{obs}}{\tau_r} \tag{Eq. 1}$$

where k_r, k_{nr}, τ_{obs} and τ_r are the radiative and non-radiative rate constants, observed and radiative lifetimes, respectively. This assumes that only radiative and non-radiative pathways are responsible for the depopulation of the $^5D_0$ state. Assuming the energy and dipole strength of the $^5D_0\rightarrow^7F_1$ transition is constant, it is possible to estimate the radiative lifetime from:

$$\frac{1}{\tau_r} = A_{MD} n^3 \left(\frac{I_{tot}}{I_{MD}}\right) \tag{Eq. 2}$$

where A_{MD} is the spontaneous emission probability for the $^5D_0\rightarrow^7F_1$ transition *in vacuo*, n is the refractive index of the medium and ($I_{\text{tot}}/I_{\text{MD}}$) is the ratio of the integrated area for the Eu^{3+} emission spectrum to the integrated area for the $^5D_0\rightarrow^7F_1$ transition. Taking the refractive index as $n = 1.5$,[61] we find Φ_{LS} to be 14% for **Eu-Naph** and 31% for **Eu-Biphen**, indicating that population of the Eu^{III} $^5D_0$ level *via* ligand sensitization from the naphthalene- or biphenyl-phosphonate ligands is significantly more efficient than direct excitation of the Eu^{III} center.

Quenching of Ln^{III} lifetimes by coordinated water molecules occurs as a result of non-radiative deactivation of the emissive state due to coupling with O-H oscillations.[65] The number of water molecules (n_w) in the Eu^{III} first coordination sphere can be determined with the empirical formula:[31,66]

$$n_w = 1.11 \times [\tau^{-1} - k_r - 0.31] \tag{Eq.3}$$

The n_w values calculated for **Eu-Naph** and **Eu-Biphen** of ~2 and ~0, respectively, are in excellent agreement with our constitutional and structural assignment for these materials. We

note that for **Eu-Biphen**, a slightly elevated $n_w \approx 0.5$ is obtained upon direct excitation, which suggests the contribution of additional non-radiative deactivation channels in this material. For **Eu-Bu^t**, we determined $n_w \approx 1.3$, which reflects that this compound contains both a constitutional water molecule and also contains multiple partially-protonated organophosphonate ligands which supply additional O-H oscillators.

Although it was not possible to determine Φ_{PL} or τ_{obs} with our experimental set-up for the Nd-phosphonate series, we note that relatively intense NIR emission was observed under moderate experimental conditions (7-10 and 7-10 nm excitation and emission slit widths, respectively), despite the propensity for non-radiative quenching through C-H, C-C and O-H oscillations on the ligands and coordinated water molecules.[67,68]

Table 2. Observed emission lifetime (determined from either mono- or bi-exponential decay functions) (τ_i), pre-exponential coefficients (A_i), radiative rate constants (k_r) non-radiative rate constants (k_{nr}) absolute emission quantum yields (Φ_{PL}) and calculated emission quantum yield for ligand sensitization (Φ_{LS}) and number of water molecules in the first coordination sphere (n_w) for Eu^{III}- and Tb^{III}-phosphonates.

Compound	λ_{ex} (nm)	τ_1 (ms)	A_1	τ_2 (ms)	A_2	k_r (s^{-1})	k_{nr} (s^{-1})	Φ_{PL} (%)	Φ_{LS} (%)[e]	n_w
Eu-Bu^t	393[a]	0.32 ± 0.05	0.93	1.32 ± 0.05	0.07	270	1525	3	-	1.3
Eu-Naph	393[a]	0.37 ± 0.05	1.00	-	-	359	2457	2	-	2.3
	330[b]	0.36 ± 0.05	1.00	-	-	390	2427	-	14	2.3
Eu-Biphen	393[a]	0.30 ± 0.05	0.20	1.00 ± 0.05	0.80	440	780	0.7	-	0.5
	305[c]	0.32 ± 0.05	0.23	1.32	0.73	252	717	-	31	0.2
Tb-Bu^t	377[d]	0.98 ± 0.05	0.57	2.69 ± 0.05	0.47	-	-	8	-	
Tb-Biphen	377[d]	0.38 ± 0.05	0.51	0.86 ± 0.05	0.49	-	-	f	-	
	305[c]	0.33 ± 0.05	0.52	0.80 ± 0.05	0.48	-	-	-	-	

[a] λ_{ex} = 393 nm ($^7F_0 \leftarrow {}^5L_6$), [b] λ_{ex} = 330 nm (Naph excitation), [c] λ_{ex} = 305 nm (Biphen excitation), [d] λ_{ex} = 377 nm ($^5D_3 \leftarrow {}^7F_6$), [e] Φ_{LS} calculated using the average experimental lifetime $\langle\tau\rangle = \Sigma\tau_iA_i^2/\tau_iA_i$ and corrected emission spectrum for Eu^{III}, [f] measured emission intensities too low to determine Φ_{PL}. N.B no emission lifetimes or quantum yields measured for **Tb-Naph** due to absence of room-temperature photoluminescence.

4. Discussion

A combination of powder and single-crystal X-ray diffraction studies were employed to investigate the influence of size, shape and steric effects of the organic ligand on the dimensionality and supramolecular organization in layered lanthanide phosphonates. The observed *d*-spacings are in excellent agreement with the length of the organic ligands incorporated, whereby organic moieties from two adjacent layers are accommodated into the

interlamellar space. We have seen that size and shape of the ligand can have an effect on the type of layered phosphonate that forms. In **Ln-Bu^t** materials, the ***t*-BuPO$_3$H$_2$** ligand size determines the ligand to metal ratio in the compound and to maintain charge balance, one of the phosphonate oxygen donors remains protonated and does not bridge between metal centers. This binding mode results in a one dimensional polymer. Water of crystallization is present to help stabilize these chains by the formation of hydrogen bonding between chains and the protonated oxygen atom allowing the formation of a pleated layer. In contrast, **Ln-Naph** and **Ln-Biphen** materials form the more familiar layered structures, similar to the previously reported lanthanide phenyl phosphonates. As confirmed by TGA and PL spectroscopy, in **Ln-Naph** two water molecules coordinate directly to the metal center, whereas in **Ln-Biphen** there is no water present. It seems plausible to attribute this effect to differences in the size and nature of the two ligands, whereby the steric bulk of the **Naph-PO$_3$H$_2$** moiety augments the coordination space around the Ln^{III} center, facilitating the direct coordination of the smaller water molecules.

Ln-phosphonates exhibit two distinct morphologies; 2D plates and 1D nanorods. We observe that a smaller ionic radius (*i.e.* Yb^{III}) favors one-dimensional growth, which is consistent with the nanomorphology reported previously for layered lanthanide phosphates (LnPO$_4$) and lanthanide hydroxides (Ln(OH)$_3$).[60] Moreover Ln-Bu^t materials, in particular, exhibit rod-like crystal morphologies with a high aspect ratio, which is in excellent agreement with the formation of a 1D coordination polymer that assembles in the solid-state *via* hydrogen bonding into a *pseudo*-2D supramolecular structure, as identified by X-ray crystallography. The anisotropy of these interactions that prevail in distinct directions of space is thus reflected in the crystal habit.

The addition of STS generally leads to more uniform crystal morphologies, improving the sample monodispersity. The influence of STS was previously considered in nanorod

growth in lanthanide phenyl phosphonates.[54] Two growth mechanisms were proposed. In the first, the formation of an intercalated structure where STS molecules are held between the hydrophobic lamellar phase of the lanthanide phenyl phosphonate is described; subsequent removal of the STS exfoliates the structure into the individual nanorods. The second mechanism postulates that 1D crystal growth is possible if the chemical potential of the monomers in solution are higher than the chemical potential of an atom on a crystal seed. Since we observed one-dimensional crystal growth even in the absence of STS, we believe that for Ln-Bu^t the connectively of individual lanthanide phosphonate centers plays a more critical role in defining the crystal morphology.

With the exception of **Yb-Naph**, which forms rod-like structures, irregular two-dimensional plates are more commonly observed for Ln-Naph materials. Considering this, it is likely that there is no or only a small anisotropic structural feature from the ligand-lanthanide bonding within the layer, so preferential favored one-dimensional growth is reduced or even absent. The Ln-Biphen series is influenced by the more extended hydrophobic ligand, which gives rise to film-like assemblies, whose amorphous character is consistent with the corresponding PXRD patterns.

The photoluminescence characterization of the Eu^{III}-phosphonates enabled us to investigate not only the optical properties of these materials, but also provided complementary insight into the molecular structure, which was crucial for those systems where it was not possible to obtain single crystal X-ray diffraction data. Firstly, the observation of a single component for the $^5D_0 \rightarrow {}^7F_0$ transition confirms that there is only one unique crystallographic site in each material.[29,62] Secondly, for **Eu-Naph**, splitting of the $^7F_1 \rightarrow {}^5D_0$ transition into three Stark components supports the unit cell assignment as orthorhombic.[69] Furthermore, splitting of the $^7F_2 \rightarrow {}^5D_0$ into only three Stark components suggests a point group symmetry close to D_2 indicating the coordination environment around

the Eu^{III}-center is likely a distorted dodecahedron.[69] Moreover, the number of water molecules estimated from time-resolved PL measurements for **Eu-Bu^t**, **Eu-Naph** and **Eu-Bibphen** (n_w = 1, 2 and 0, respectively) was in excellent agreement with that obtained from TGA and/or X-ray crystallography.

With the exception of **Tb-Naph**, room temperature photoluminescence is observed *via* both direct excitation of the Ln^{III} center and ligand sensitization for all Ln-phosphonates studied. Near-infrared (NIR) emission was observed from both Nd- and Yb-phosphonates at room temperature, *via* both direct excitation and ligand sensitization. We note that emission quantum yields obtained for direct excitation of Eu-phosphonates (Φ_{PL} ~0.7, 2 and 3% for **Eu-Biphen**, **Eu-Naph** and **Eu-Bu^t**, respectively) are lower than those previously reported for Eu^{III}-doped La^{III} phenyl phosphonates (e.g. Φ_{PL} = 10% for $La(HO_3PC_6H_5)_2$:0.06Eu).[55] This is attributed to enhanced concentration quenching in our Ln-phosphonate materials, whereby excitation energy transfer between nearest neighbor Eu^{III} lattice sites activates an additional non-radiative deactivation channel.[70] Emission quantum yields for ligand sensitization, Φ_{LS}, are considerably higher than direct excitation (Φ_{LS} =14% and Φ_{LS} = 31% for **Eu-Naph** and **Eu-Biphen**, respectively). Ligand sensitization proceeds *via* energy transfer from the lowest excited triplet state (T_1) of the ligand antenna. It has been previously demonstrated that energy transfer occurs most efficiently when an energy gap of ΔE = 2500-3000 cm^{-1} between the triplet donor state on the ligand and the emissive state of the acceptor Ln^{III} center is present.[49,71] The triplet state energies were estimated from the 77 K phosphorescence spectra and were found to be 21,097 cm^{-1} for 1-naphthalene phosphonic acid and 22,624 cm^{-1} for 4-biphenyl phosphonic acid, respectively (Figure S7b,d, Supporting Information). Figure 6 shows the corresponding energy level diagram for **Ln-Naph** and **Ln-Biphen** (Ln = Eu^{III}, Tb^{III}). For Eu^{III}-phosphonates the T_1 energies of both organic ligands lie ~3500-4500 cm^{-1} above the emissive $^5D_0$ manifold (~17400 cm^{-1}), resulting in good energy transfer. For **Tb-**

Naph no room-temperature PL was observed. Examination of the energy level diagram reveals that the Naph T_1 state lies ~600 cm^{-1} above the emissive $^5D_4$ state (20,490 cm^{-1}). At room temperature, thermal population of higher vibrational levels within the $^5D_4$ manifold is expected, thus facilitating back energy transfer to the ligand. However, on cooling to 77 K, the characteristic Tb^{III} emission spectrum is observed for **Tb-Naph**, suggesting that the probability for back energy transfer to the ligand T_1 level is reduced due to a decreased Boltzmann population of vibrational levels. In contrast for **Tb-Biphen**, the ligand T_1 state lies ~2100 cm^{-1} above the Tb^{III} emissive state, resulting in efficient ligand to metal energy transfer and inhibiting back energy transfer at room temperature. This indicates that with judicious matching of the ligand donor and Ln^{III} acceptor energy levels it is possible to switch the Ln^{III} photoluminescence on and off by changing the temperature.
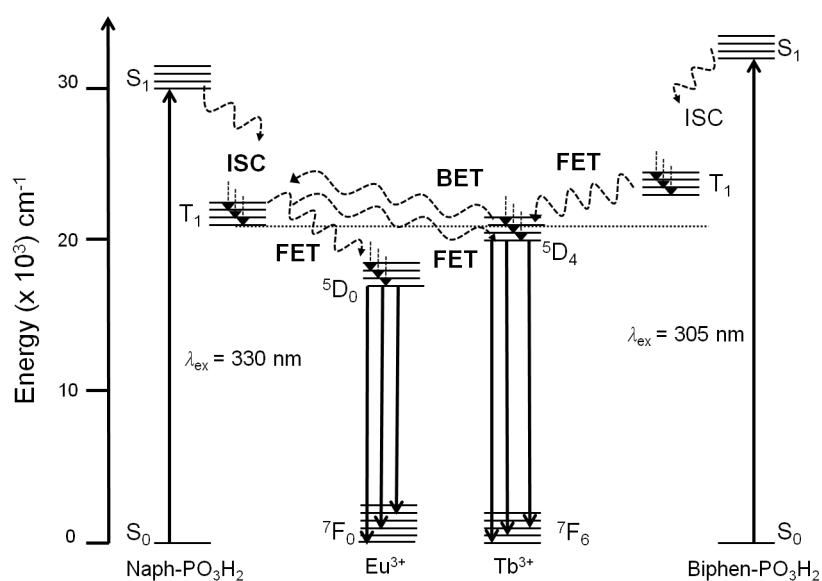
Figure 6. Partial energy level diagram of 1-naphthalene- and 4-biphenyl-phosphonic acids (Naph-PO$_3$H$_2$ and Biphen-PO$_3$H$_2$, respectively) and Eu^{III} (intra-4f^6) and Tb^{III} (intra-4f^8) energy levels. Solid and dashed lines represent radiative and non-radiative transitions, respectively. ISC – intersystem crossing, FET – forward energy transfer, BET – back energy transfer.

Conclusions

In this work, we have synthesized and characterized the structure, morphology and photoluminescence properties of a series of two-dimensional, layered Ln^{III}-phosphonate materials. Through systematic variation of the ligand (Bu^t-PO$_3$H$_2$, Naph-PO$_3$H$_2$ and Biphen-PO$_3$H$_2$) and Ln^{III} (Eu^{III}, Tb^{III}, Nd^{IIII} and Yb^{III}) incorporated, we have been able to identify the key structure-property relationships that control the supramolecular organization, morphology and optical properties of unprecedented organic-inorganic hybrid Ln-phosphonates. The small, saturated ligand Bu^t-PO$_3$H$_2$ within the corresponding **Ln-Bu^t series**, promotes the growth of 1D coordination polymers, which are assembled into *pseudo*-two-dimensional sheets *via* hydrogen bonding. We report the crystallographic structure of these materials here for the first time. The anisotropy of the primary building units is reflected in the tendency of **Ln-Bu^t** to adopt nanoscopic rodlike crystal morphologies. In contrast, larger aromatic ligands bridge directly between Ln^{III} centers, forming 2D, layered materials in which the interlamellar distance may be tuned by the ligand size. **Ln-Naph** and **Ln-Biphen** materials typically result in a 2D platelike crystal morphology or form amorphous films. With the exception of **Tb-Naph**, all Ln^{III}-phosphonates exhibit room temperature photoluminescence that is characteristic of the nature of the incorporated Ln^{III} ion. The emission efficiency can be modulated through judicious selection of the organic ligand: aromatic ligands such as Naph-PO$_3$H$_2$ and Biphen-PO$_3$H$_2$ facilitate population of the Ln^{III} emissive state *via* ligand sensitization, resulting in increased emission quantum yields. However, if the energy gap between the ligand T$_1$ donor level and the Ln^{III} acceptor state is too small (<1000 cm^{-1}), reverse energy transfer can inhibit photoluminescence at room temperature, as observed for **Tb-Naph**. Lowering the temperature, however, can result in the PL channel being switched on once again. Careful consideration of both the ligand and Ln^{III} energy level diagrams should thus be essential step when designing emissive, Ln-

phosphonate materials. This study therefore provides key insight into the essential structure-property relationships that must be identified for the design of layered, organic-inorganic materials with tailored functionality and morphology.

Acknowledgements

Supporting Information Available

Ligand and Ln-phosphonate synthesis, additional structural characterisation data (FTIR spectra, TGA data, PXRD patterns and crystallographic data, supporting PL spectra and emission decay curves. Experimental conditionsThis information is available free of charge via the Internet at http://pubs.acs.org

References

(1)   Clearfield, A. Recent Advances in Metal Phosphonate Chemistry. *Curr. Opin. Solid State Mater. Sci.* **1996**, *1*, 268-278.

(2)   Clearfield, A. Advances in Metal Phosphonate Chemistry II. *Curr. Opin. Solid State Mater. Sci.* **2002**, *6*, 495-506.

(3)   Zhang, Y. B.; Tan, Y. W.; Stormer, H. L.; Kim, P. Experimental Observation of the Quantum Hall Effect and Berry's Phase in Graphene. *Nature* **2005**, *438*, 201-204.

(4)   Balandin, A. A.; Ghosh, S.; Bao, W. Z.; Calizo, I.; Teweldebrhan, D.; Miao, F.; Lau, C. N. Superior Thermal Conductivity of Single-layer Graphene. *Nano Lett.* **2008**, *8*, 902-907.

(5)   Bonaccorso, F.; Sun, Z.; Hasan, T.; Ferrari, A. C. Graphene Photonics and Optoelectronics. *Nature Photon.* **2010**, *4*, 611-622.

(6)   Radisavljevic, B.; Radenovic, A.; Brivio, J.; Giacometti, V.; Kis, A. Single-Layer MoS_2 Transistors. *Nature Nanotechnol.* **2011**, *6*, 147-150.

(7)   Eda, G.; Yamaguchi, H.; Voiry, D.; Fujita, T.; Chen, M. W.; Chhowalla, M. Photoluminescence from Chemically Exfoliated MoS_2. *Nano Lett.* **2011**, *11*, 5111-5116.

(8)   Sundaram, R. S.; Engel, M.; Lombardo, A.; Krupke, R.; Ferrari, A. C.; Avouris, P.; Steiner, M. Electroluminescence in Single Layer MoS_2. *Nano Lett.* **2013**, *13*, 1416-1421.

(9)   Shanmugam, M.; Jacobs-Gedrim, R.; Durcan, C.; Yu, B. 2D Layered Insulator Hexagonal Boron Nitride Enabled Surface Passivation in Dye Sensitized Solar Cells. *Nanoscale* **2013**, *5*, 11275-11282.

(10)   Pakdel, A.; Zhi, C. Y.; Bando, Y.; Nakayama, T.; Golberg, D. Boron Nitride Nanosheet Coatings with Controllable Water Repellency. *ACS Nano* **2011**, *5*, 6507-6515.

(11)   Fong, C. Y.; Ng, S. S.; Yam, F. K.; Abu Hassan, H.; Hassan, Z. Synthesis of Two-Dimensional Gallium Nitride *via* Spin Coating Method: Influences of Nitridation Temperatures. *J. Sol-Gel Sci. Technol.* **2013**, *68*, 95-101.

(12)   Breen, J. M.; Schmitt, W. Hybrid Organic-Inorganic Polyoxometalates: Functionalization of V^{IV}/V^V Nanosized Clusters to Produce Molecular Capsules. *Angew. Chem. Int. Ed.* **2008**, *47*, 6904-6908.

(13)   Onet, C. I.; Zhang, L.; Clerac, R.; Jean-Denis, J. B.; Feeney, M.; McCabe, T.; Schmitt, W. Self-Assembly of Hybrid Organic-Inorganic Polyoxomolybdates: Solid-State Structures and Investigation of Formation and Core Rearrangements in Solution. *Inorg. Chem.* **2011**, *50*, 604-613.

(14)   Zhang, L.; Clerac, R.; Onet, C. I.; Venkatesan, M.; Heijboer, P.; Schmitt, W. Supramolecular Approach by Using Jahn-Teller Sites to Construct a $\{Mn_{13}\}$-Based Coordination Polymer and Modify its Magnetic Properties. *Chem. Eur. J.* **2012**, *18*, 13984-13988.

(15)   Zhang, L.; Clerac, R.; Heijboer, P.; Schmitt, W. Influencing the Symmetry of High-Nuclearity and High-Spin Manganese Oxo Clusters: Supramolecular Approaches to Manganese-Based Keplerates and Chiral Solids. *Angew. Chem. Int. Ed.* **2012**, *51*, 3007-3011.

(16)   Breen, J. M.; Zhang, L.; Clement, R.; Schmitt, W. Hybrid Polyoxovanadates: Anion-Influenced Formation of Nanoscopic Cages and Supramolecular Assemblies of Asymmetric Clusters. *Inorg. Chem.* **2012**, *51*, 19-21.

(17)   Breen, J. M.; Clerac, R.; Zhang, L.; Cloonan, S. M.; Kennedy, E.; Feeney, M.; McCabe, T.; Williams, D. C.; Schmitt, W. Self-Assembly of Hybrid Organic-Inorganic Polyoxovanadates: Functionalised Mixed-Valent Clusters and Molecular Cages. *Dalton Trans.* **2012**, *41*, 2918-2926.

(18)   Zhang, L.; Marzec, B.; Clerac, R.; Chen, Y. H.; Zhang, H. Z.; Schmitt, W. Supramolecular Approaches to Metal-Organic Gels Using 'Chevrel-Type' Coordination Clusters as Building Units. *Chem. Commun.* **2013**, *49*, 66-68.

(19)   Zhang, L.; Clerac, R.; Onet, C. I.; Healy, C.; Schmitt, W. Towards Nanoscopic Mn-Containing Hybrid Polyoxomolybdates: Synthesis, Structure, Magnetic Properties and Solution Behavior of a $\{Mn_6Mo_{10}\}$ Cluster. *Eur. J. Inorg. Chem.* **2013**, *10-11*, 1654-1658.

(20)   Papadaki, M.; Demadis, K. D. Structural Mapping of Hybrid Metal Phosphonate Corrosion Inhibiting Thin Films. *Comments Inorg. Chem.* **2009**, *30*, 89-118.

(21)   Singh, S.; Patel, P.; Shahi, V. K.; Chudasama, U. Pb^{2+} Selective and Highly Cross-Linked Zirconium Phosphonate Membrane by Sol-Gel in Aqueous Media for Electrochemical Applications. *Desalination* **2011**, *276*, 175-183.

(22)   Lin, X. Z.; Yuan, Z. Y. Synthesis of Mesoporous Zirconium Organophosphonate Solid-Acid Catalysts. *Eur. J. Inorg. Chem.* **2012**, *16*, 2661-2664.

(23)   Wang, R. C.; Zhang, Y. P.; Hu, H. L.; Frausto, R. R.; Clearfield, A. Preparation of Lanthanide Arylphosphonates and Crystal-Structures of Lanthanum Phenyl- and Benzylphosphonates. *Chem. Mater.* **1992**, *4*, 864-871.

(24)   Evans, O. R.; Ngo, H. L.; Lin, W. B. Chiral Porous Solids Based on Lamellar Lanthanide Phosphonates. *J. Am. Chem. Soc.* **2001**, *123*, 10395-10396.

(25)   Ngo, H. L.; Lin, W. B. Chiral Crown Ether Pillared Lamellar Lanthanide Phosphonates. *J. Am. Chem. Soc.* **2002**, *124*, 14298-14299.

(26)   Ying, S. M.; Zeng, X. R.; Fang, X. N.; Li, X. F.; Liu, D. S. Synthesis, Crystal Structure and Fluorescent Characterization of a Novel Lanthanide Tetraphosphonate with a Layered Structure. *Inorg. Chim. Acta* **2006**, *359*, 1589-1593.

(27)   Avecilla, F.; Peters, J. A.; Geraldes, C. X-ray Crystal Structure of a Sodium Salt of $[Gd(DOTP)]^{5-}$: Implications for its Second-Sphere Relaxivity and the ^{23}Na NMR Hyperfine Shift Effects of $[Tm(DOTP)]^{5-}$. *Eur. J. Inorg. Chem.* **2003**, *23*, 4179-4186.

(28)   Evans, R. C.; Carlos, L. D.; Douglas, P.; Rocha, J. Tuning the Emission Colour in Mixed Lanthanide Microporous Silicates: Energy Transfer, Composition and Chromaticity. *J. Mater. Chem.* **2008**, *18*, 1100-1107.

(29)   Eliseeva, S. V.; Bunzli, J. C. G. Lanthanide Luminescence for Functional Materials and Bio-Sciences. *Chem. Soc. Rev.* **2010**, *39*, 189-227.

(30)   Evans, R. C.; Ananias, D.; Douglas, A.; Douglas, P.; Carlos, L. D.; Rocha, J. Energy Transfer and Emission Decay Kinetics in Mixed Microporous Lanthanide Silicates with Unusual Dimensionality. *J. Phys. Chem. C* **2008**, *112*, 260-268.

(31)   Carlos, L. D.; Ferreira, R. A. S.; Bermudez, V. D.; Ribeiro, S. J. L. Lanthanide-Containing Light-Emitting Organic-Inorganic Hybrids: A Bet on the Future. *Adv. Mat.* **2009**, *21*, 509-534.

(32)   Rocha, J.; Carlos, L. D.; Paz, F. A. A.; Ananias, D. Luminescent Multifunctional Lanthanide-based Metal-Organic Frameworks. *Chem. Soc. Rev.* **2011**, *40*, 926-940.

(33)   Carlos, L. D.; Ferreira, R. A. S.; Bermudez, V. D.; Julian-Lopez, B.; Escribano, P. Progress on Lanthanide-based Organic-Inorganic Hybrid Phosphors. *Chem. Soc. Rev.* **2011**, *40*, 536-549.

(34)   Allendorf, M. D.; Bauer, C. A.; Bhakta, R. K.; Houk, R. J. T. Luminescent Metal-Organic Frameworks *Chem. Soc. Rev.* **2009**, *38*, 1330-1352.

(35)   Mao, J. G. Structures and Luminescent Properties of Lanthanide Phosphonates. *Coord. Chem. Rev.* **2007**, *251*, 1493-1520.

(36)   Serre, C.; Stock, N.; Bein, T.; Ferey, G. Synthesis and Characterization of a New Three-Dimensional Lanthanide Carboxyphosphonate: $Ln_4(H_2O)_7[O_2C-C_5H_{10}N-CH_2-PO_3]_4(H_2O)_5$. *Inorg. Chem.* **2004**, *43*, 3159-3163.

(37)   Tang, S. F.; Song, J. L.; Mao, J. G. Syntheses, Crystal Structures and Characterizations of a Series of New Layered Lanthanide Carboxylate-Phosphonates. *Eur. J. Inorg. Chem.* **2006**, *10*, 2011-2019.

(38)   Yue, Q.; Yang, J.; Li, G. H.; Li, G. D.; Chen, J. S. Homochiral Porous Lanthanide Phosphonates with 1D Triple-Strand Helical Chains: Synthesis, Photoluminescence and Adsorption Properties. *Inorg. Chem.* **2006**, *45*, 4431-4439.

(39)   Tang, S. F.; Song, J. L.; Li, X. L.; Mao, J. G. Luminescent Lanthanide(III) Carboxylate-Phosphonates with Helical Tunnels. *Cryst. Growth Des.* **2006**, *6*, 2322-2326.

(40)   Cao, D. K.; Li, Y. Z.; Song, Y.; Zheng, L. M. Three-, Two-, and One-Dimensional Metal Phosphonates Bbased on [Hydroxy(4-pyridyl)methyl]phosphonate: $M\{(4-C_5H_4N)CH(OH)PO_2\}_3 \cdot 6H_2O$ (M = Ni, Cd) and $Gd\{(4-C_5H_4N)CH(OH)P(OH)O_2\}_3 \cdot 6H_2O$. *Inorg. Chem.* **2005**, *44*, 3599-3604.

(41)   Nash, K. L.; Rogers, R. D.; Ferraro, J.; Zhang, J. Lanthanide Complexes with 1-hydroxyethane-1,1-diphosphonic acid: Solvent Organization and Coordination Geometry in Crystalline and Amorphous Solids. *Inorg. Chim. Acta* **1998**, *269*, 211-223.

(42)   Glowiak, T.; Huskowska, E.; Legendziewicz, J. Preparation and X-ray Crystal Structure Determination of an Octahedral Polymeric Lutetium Compound with Ciliatine; $\{Lu(PO_3HCH_2CH_2NH_3)_3(ClO_4)_3 \cdot 3D_2O\}n$. *Polyhedron* **1991**, *10*, 175-178.

(43)   Groves, J. A.; Stephens, N. F.; Wright, P. A.; Lightfoot, P. Novel Open-Framework Architectures in Lanthanide Phosphonates. *Solid State Sci.* **2006**, *8*, 397-403.

(44)   Plutnar, J.; Rohovec, J.; Kotek, J.; Zak, Z.; Lukes, I. Novel Polymeric Metal Complexes of Calix[4]arene-11,23-diphosphonic acid: Synthesis and Structure Determination. *Inorg. Chim. Acta* **2002**, *335*, 27-35.

(45)   Rudovsky, J.; Cigler, P.; Kotek, J.; Hermann, P.; Vojtisek, P.; Lukes, I.; Peters, J. A.; Vander Elst, L.; Muller, R. N. Lanthanide(III) Complexes of a Mono(methylphosphonate) Analogue of H_4dota: The Influence of Protonation of the Phosphonate Moiety on the TSAP/SAP Isomer Ratio and the Water Exchange Rate. *Chem.-Eur. J.* **2005**, *11*, 2373-2384.

(46)   Bünzli, J.-C. G.; Eliseeva, S. V. In *Springer Series on Fluorescence, Vol. 7, Lanthanide Luminescence*; Hänninen, P., Härmä, H.; Springer Verlag: Berlin, 2010; p 1.

(47)   Weissman, S. I. Intramolecular Energy Transfer: The Fluorescence of Complexes of Europium *J. Chem. Phys.*, **1942**, *10*, 214-217.

(48)   Klink, S. I.; Grave, L.; Reinhoudt, D. N.; van Veggel, F.; Werts, M. H. V.; Geurts, F. A. J.; Hofstraat, J. W. A Systematic Study of the Photophysical Processes in Polydentate Triphenylene-Functionalized Eu^{3+}, Tb^{3+}, Nd^{3+}, Yb^{3+}, and Er^{3+} Complexes. *J. Phys. Chem. A* **2000**, *104*, 5457-5468.

(49)   Samuel, A. P. S.; Xu, J. D.; Raymond, K. N. Predicting Efficient Antenna Ligands for Tb(III) Emission. *Inorg. Chem.* **2009**, *48*, 687-698.

(50)   Zhang, H. B.; Peng, Y.; Shan, X. C.; Tian, C. B.; Ping, L.; Du, S. W. Lanthanide Metal Organic Frameworks Based on Octahedral Secondary Building Units: Structural, Luminescent and Magnetic Properties. *Inorg. Chem. Commun.* **2011**, *14*, 1165-1169.

(51)   Lin, Z. J.; Xu, B.; Liu, T. F.; Cao, M. N.; Lu, J. A.; Cao, R. A Series of Lanthanide Metal-Organic Frameworks Based on Biphenyl-3,4 ',5-tricarboxylate: Syntheses, Structures, Luminescence and Magnetic Properties. *Eur. J. Inorg. Chem.* **2010**, *24*, 3842-3849.

(52)   Comby, S.; Scopelliti, R.; Imbert, D.; Charbonniere, L.; Ziessel, R.; Bunzli, J. C. G. Dual Emission from Luminescent Nonalanthanide Clusters. *Inorg. Chem.* **2006**, *45*, 3158-3160.

(53)   Du, Z. Y.; Xu, H. B.; Mao, J. G. Rational Design of 0D, 1D, and 3D Open Frameworks Based on Tetranuclear Lanthanide(III) Sulfonate-Phosphonate Clusters. *Inorg. Chem.* **2006**, *45*, 9780-9788.

(54)   Song, S. Y.; Ma, J. F.; Yang, J.; Cao, M. H.; Zhang, H. J.; Wang, H. S.; Yang, K. Y. Systematic Synthesis and Characterization of Single-Crystal Lanthanide Phenylphosphonate Nanorods. *Inorg. Chem.* **2006**, *45*, 1201-1207.

(55)   Di, W. H.; Ferreira, R. A. S.; Willinger, M. G.; Ren, X. G.; Pinna, N. Enhanced Photoluminescence Features of Rare Earth Phenylphosphonate Hybrid Nanostructures Synthesized under Nonaqueous Conditions. *J. Phys. Chem. C* **2010**, *114*, 6290-6297.

(56)   Di, W. H.; Ren, X. G.; Shirahata, N.; Liu, C. X.; Zhang, L. G.; Sakka, Y.; Pinna, N. Hybrid Dandelion-like $YH(O_3PC_6H_5)_2$:Ln (Ln = Eu^{3+}, Tb^{3+}) Particles: Formation Mechanism, Thermal and Photoluminescence Properties. *CrystEngComm* **2011**, *13*, 5226-5233.

(57)   Sheldrick G. M. *SHELXTL*, version 5.1; Bruker-AXS Inc.: Madison, WI, 1999.

(58)   Aspinall, H. C.; Bickley, J. F.; Dwyer, J. L. M.; Greeves, N.; Kelly, R. V.; Steiner, A. Pinwheel-Shaped Heterobimetallic Lanthanide Alkali Metal Binaphtholates: Ionic Size Matters! *Organometallics* **2000**, *19*, 5416-5423.

(59)   Bretonniere, Y.; Mazzanti, M.; Pecaut, J.; Olmstead, M. M. Cation-Controlled Self-Assembly of a Hexameric Europium Wheel. *J. Am. Chem. Soc.* **2002**, *124*, 9012-9013.

(60)   Wang, G. F.; Peng, Q.; Li, Y. D. Lanthanide-Doped Nanocrystals: Synthesis, Optical-Magnetic Properties and Applications. *Acc. Chem. Res.* **2011**, *44*, 322-332.

(61)   Vilela, S. M. F.; Ananias, D.; Gomes, A. C.; Valente, A. A.; Carlos, L. D.; Cavaleiro, J. A. S.; Rocha, J.; Tome, J. P. C.; Paz, F. A. A. Multi-Functional Metal-Organic Frameworks Assembled from a Tripodal Organic Linker. *J. Mater. Chem.* **2012**, *22*, 18354-18371.

(62)   Muller, G.; Kean, S. D.; Parker, D.; Riehl, J. P. Temperature and Pressure Dependence of Excitation Spectra as a Probe of the Solution Structure and Equilibrium Thermodynamics of a Eu(III) Complex Containing a Modified dota Ligand. *J. Phys. Chem. A* **2002**, *106*, 12349-12355.

(63)   Werts, M. H. V.; Jukes, R. T. F.; Verhoeven, J. W. The Emission Spectrum and the Radiative Lifetime of Eu^{3+} in Luminescent Lanthanide Complexes. *Phys. Chem. Chem.Phys.* **2002**, *4*, 1542-1548.

(64) Blasse, G.; Grabmaier, B. C.; In *Luminescent Materials*, Springer-Verlag, **1994**, Chapter 4.

(65)   Lis, S. Luminescence Spectroscopy of Lanthanide(III) Ions in Solution. *J. Alloys Compd.* **2002**, *341*, 45-50.

(66)   Supkowski, R. M.; Horrocks, W. D. On the Determination of the Number of Water Molecules, *q*, Coordinated to Europium(III) Ions in Solution from Luminescence Decay Lifetimes. *Inorg. Chim. Acta* **2002**, *340*, 44-48.

(67)   Tan, R. H. C.; Motevalli, M.; Abrahams, I.; Wyatt, P. B.; Gillin, W. P. Quenching of IR Luminescence of Erbium, Neodymium and Ytterbium Beta-Diketonate Complexes by Ligand C-H and C-D Bonds. *J. Phys. Chem. B* **2006**, *110*, 24476-24479.

(68)   Blasse, G.; Sabbatini, N. The Quenching of Rare-Earth Ion Luminescence in Molecular and Nonmolecular Solids. *Mater. Chem. Phys.* **1987**, *16*, 237-252.

(69)   Binnemans, K.; Gorller-Walrand, C. Application of the Eu^{3+} Ion for Site Symmetry Determination. *J. Rare Earth* **1996**, *14*, 173-180.

(70)   Xue, N.; Fan, X. P.; Wang, Z. Y.; Wang, M. Q. Synthesis Process and Luminescence Properties of Ln^{3+} doped $NaY(WO_4)_2$ Nanoparticles. *Mater. Lett.* **2007**, *61*, 1576-1579.

(71)   Latva, M.; Takalo, H.; Mukkala, V. M.; Matachescu, C.; Rodriguez-Ubis, J. C.; Kankare, J. Correlation between the Lowest Triplet State Energy Level of the Ligand and Lanthanide(III) Luminescence Quantum Yield. *J. Lumin.* **1997**, *75*, 149-169.

Table of Contents

2D Layered Ln(III)
Phosphonates

Vary Ln (III)

Vary Phosphonic
Acid

Tune Photoluminescence

Switch on Energy Transfer

Control Aspect Ratio